Surface-modified graphene nanosheets for anticancer drug delivery

표면수식 그래핀 나노시트를 이용한 항암제 전달 연구

2015년 8월

서울대학교 융합과학기술대학원

분자의학 및 바이오제약학과

한 정 훈

Abstract

Surface-modified graphene nanosheets for anticancer drug delivery

Jeonghoon Han

Molecular Medicine and Biopharmaceutical Sciences

WCU Graduate School of Convergence Science and Technology

Seoul National University

Here, we report reduced graphene oxide (rGO) nanosheets coated with an anti-angiogenic anticancer taurocholate derivative of low-molecular-weight heparin (LHT7) as a tumor-targeting nanodelivery platform for anticancer drugs. Surface coating of LHT7 onto rGO was confirmed using fluorescein isothiocyanate-labeled LHT7, monitored as fluorescence quenching due to associated rGO. Unlike plain rGO, LHT7-coated rGO (LHT-rGO) nanosheets maintained a stable dispersion under physiological conditions for at least 24 h. Moreover, LHT-rGO provided greater loading capacity for doxorubicin (Dox) compared with uncoated rGO nanosheets. Following intravenous administration into KB tumor-bearing mice, in vivo tumor accumulation of LHT-rGO/Dox was 7-fold higher than that of rGO/Dox 24 h post dosing. Intravenously administered LHT-rGO/Dox showed the greatest anti-tumor effect in KB-bearing mice, reducing tumor volume by $92.5\% \pm 3.1\%$ compared to the untreated group 25 days after tumor inoculation. TUNEL assays revealed that the population of apoptotic cells was highest in the group treated with LHT-rGO/Dox. Taken together, our results demonstrate that LHT-rGO nanosheets confer improved dispersion stability, tumor distribution and *in vivo* antitumor

effects, and may be further developed as a potential active nanoplatform of various anticancer drugs.

Key words: anti-angiogenic anticancer low molecular weight heparin derivative, reduced graphene oxide, dispersion stability, doxorubicin, anticancer effect.

Contents

1. Introduction

2. Materials and methods

3. Results

4. Discussion

5. Conclusion

References

국문초록

List of Figures

1. Introduction

Graphene-based nanomaterials have been the focus of considerable research efforts by virtue of their unique features, including optical, mechanical, chemical and thermal properties, raising tremendous interest for their potential pharmaceutical applications[1-3]. However, because graphene-based nanosheets are derived from hydrophobic graphite through chemical or physical modification, their pharmaceutical applications have been hampered by their instability under physiological conditions [4-8].

Reduced graphene oxide (rGO) nanosheets that mimic single-layered graphene nanosheets have been generated by decreasing the polar groups on graphene oxide (GO). The planar structure of rGO serves a double-edged sword: it provides a high capacity for hydrophobic interactions among various functional molecules, but it leads to formation of aggregates with poor dispersion stability under physiological conditions[9,10].

Surface modification of rGO with synthetic polymers or biopolymers has been used to stabilize and improve the utility of rGO as nanocarriers for therapeutics[11-16]. Polyethylene glycol (PEG)-grafted rGO nanosheets have been shown to provide a high loading capacity and cellular-uptake efficiency for single-stranded RNA cargoes[12]. Functionalization of rGO with PEGylated, branched polyethylenimine has been reported to promote cytosolic drug delivery through photothermal disruption of endosomes[13]. Biopolymers, such as hyaluronic acid derivatives[14], dextran[15], and heparin[16], have been studied as surface coatings for rGO. However, most molecules used for surface coating do not possess intrinsic anticancer activity. If an rGO surface coating material were capable of providing both stabilization and anticancer effects, it might enhance the suitability of rGO for anticancer drug delivery applications.

Derivatives of low-molecular-weight heparin (LMWH), a highly sulfated polysaccharide, have been studied as potential anticancer agents[17]. Among LMWH derivatives, LMWH-taurocholate conjugate 7 (LHT7), in which LMWH is conjugated to taurocholic acid at a molar ratio of 1 to 7, has been

suggested as a prominent anticancer drug with significantly enhanced anti-angiogenic activity and reduced anti-coagulant activity[18]. Recently, liposomal co-delivery of LHT7 and suberanilohydroxamic acid, a histone deacetylase inhibitor, was shown to provide synergistic anticancer activity[19].

Taking advantage of the anti-angiogenic anticancer activity of LHT7 and its highly sulfated polysaccharide and taurocholate moieties, we hypothesized that surface coating of rGO with LHT7 would improve the dispersion stability of these nanosheets and enhance the anticancer efficacy upon delivery with a chemical anticancer drug. In this study, we thus investigated whether LHT7 affected the dispersion stability of rGO and evaluated the *in vivo* distribution and antitumor effects of LHT7-coated rGO nanosheets loaded with the anticancer drug, doxorubicin (Dox).

2. Materials and Methods

2.1. Synthesis of LHT7 and F-LHT7

LHT7 was synthesized according to a previously described method[19]. Briefly, ethylenediaminetaurocholicacid (5 g) was dissolved in methanol (150 ml) in the presence of sodiumhydroxide (5g). After stirring for 2 h, the solution was precipitated with cold acetonitrile. The resulting precipitate, sodium ethylenediamine taurocholate, was washed with cold acetonitrile and freeze-dried. Five hundred milligrams of LMWH (Fraxiparin; Nanjing King–Friend Biochemical Pharmaceutical Company Ltd., Nanjing, China) was dissolved in distilled water in the presence of N-hydroxysuccinimide (126.6 mg). Then, N-ethyl-N´-(3-dimethylaminopropyl) carbodiimide hydrochloride (310 mg) and sodium ethylenediamine taurocholate (686 mg) were added consecutively into this solution. After an overnight reaction, the solution was precipitated, washed with cold methanol, and freeze-dried. The final product, LHT7, was obtained as a white powder.

For the synthesis of fluorescein isothiocyanate (FITC)-labeled LHT7 (F-LHT7), LHT7 (200 mg) was dissolved in 0.1 M borate buffer (pH 9.0). This solution

was then mixed with 20 mg of FITC (Sigma-Aldrich Chemical Co., St. Louis, MO, USA), dissolved in anhydrous dimethyl sulfoxide (DMSO), and reacted for 5 h. The compound was washed twice with cold methanol and then dissolved in distilled water. The solution was purified by dialysis using a membrane with a molecular-weight cutoff of 2000 Da (Spectrum Laboratories Inc., Rancho Dominguez, CA, USA) and freeze-dried to yield the final product, F-LHT7.

2. 2. Preparation of rGO nanosheets

rGO nanosheets were produced by reducing GO nanosheets. GO nanosheets were prepared from graphite using Hummer's method with slight modification [14]. Briefly, graphite powder (0.5 g; Sigma-Aldrich), $KMnO_4$ (3g; Sigma-Aldrich) and $NaNO_3$ (0.5 g; Sigma-Aldrich) were added to cold H_2SO_4 (23 ml), and the mixture was stirred initially on ice and then at 35℃ for an additional 1 h. After addition of 46 ml of triple-distilled water (TDW), the mixture was stirred at 90℃ for 1 h. The reaction was stopped by addition of 140 ml of TDW and 10 ml of 30% H_2O_2. After washing, the reaction products were dispersed in TDW and sonicated for 2 h to exfoliate the GO layers and form GO nanosheets. Un-exfoliated GO was removed by centrifugation at $1600 \times$ g for 10 min. The supernatant containing GO nanosheets were collected and filtered through 0.2-μm polycarbonate membrane filters (Millipore Corp., Billerica, MA, USA) using an extruder (Northern Lipid, British Columbia, Canada).

For preparation of rGO nanosheets, the resulting GO nanosheets were reduced by adding 2.0 ml of GO nanosheets (5 mg/ml) in TDW to 8.0 ml of TDW, 0.5 ml of ammonia solution (28 w/w% in water; Junsei Chemical, Tokyo, Japan), and 5.0 μl of hydrazine monohydrate (64 w/w% in water; Sigma-Aldrich). The resulting mixture was stirred at 80℃ for 10 min. After cooling to room temperature, excess hydrazine and ammonia were removed by dialysis (molecular weight cutoff, 100 kDa; Spectrum Laboratories, Inc.) against TDW. The obtained rGO nanosheets were stored at 4℃ until use.

2. 3. Preparation and characterization of LHT-rGO nanosheets

For coating surfaces with LHT7, rGO nanosheets in TDW (1 mg/ml) were mixed with an equivalent volume of LHT7 solution (5 mg/ml) at a LHT7:rGO weight ratio of 5:1. Unloaded LHT7 was removed by gel filtration through a Sephadex G-25M column (GE Healthcare, Piscataway, NJ, USA), yielding LHT-rGO nanosheets. The extent of LHT7 loading onto rGO was determined by measuring the decrease in F-LHT7 fluorescence at 525 nm caused by the quenching of adsorbed fluorophores by rGO using a fluorescence microplate reader (Gemini XS; Molecular Device, Sunnyvale, CA, USA). The size and morphology of LHT-rGO were examined by transmission electron microscopy (JEM1010; JEOL Ltd, Tokyo, Japan).

2. 4. Stability test of LHT-rGO nanosheets

The stability of LHT-rGO nanosheets was tested in phosphate-beffered saline (PBS) (50 mM, pH 7.4) and fetal bovine serum (FBS; Gibco BRL Life Technologies, Carlsbad, CA, USA). An aliquot (0.1 ml) of rGO or LHT-rGO in TDW (rGO content, 0.5 mg/ml) was added to 0.9 ml of PBS, and the solutions were allowed to stand for 24 h. The stability of LHT-rGO nanosheets in PBS was evaluated by monitoring the mixtures for the appearance of precipitates using a digital camera (Canon PC17089; Canon Inc, Tokyo, Japan). For tests of LHT-rGO stability in serum, an aliquot (0.1 ml) of F-LHT-rGO in TDW (rGO content, 0.5 mg/ml) was added to 0.9 ml of RPMI-1640 media containing FBS (10%, 50%, or 90%), and the solutions were allowed to stand for 4 h. The stability of LHT-rGO complexes was determined by measuring the fluorescence of F-LHT7 released from LHT-rGO nanosheets using a fluorescence microplate reader (Gemini XS; Molecular Device).

2.5. Preparation of Dox-loaded nanosheets

Dox was loaded onto rGO and LHT-rGO nanosheets by physical adsorption. For drug loading, 1 ml of Dox solution (0.5 mg/ml; Sigma-Aldrich) was added

to 1 ml of rGO or LHT-rGO nanosheets in TDW and stirred for 2 h at room temperature. Free Dox was then removed using a PD-10 desalting column (GE Healthcare), yielding Dox-loaded rGO (rGO/Dox) or Dox-loaded LHT-rGO (LHT-rGO/Dox). In some experiments, the resultant rGO/Dox or LHT-rGO/Dox was further eluted by the PD-10 desalting column, and the absorbance spectrum was measured using UV-vis spectrophotometry (UV-3100, Shimadzu Corp, Tokyo, Japan). The extent of Dox loading onto rGO and LHT-rGO nanosheets was determined by measuring the loss of Dox fluorescence at 485 nm caused by the quenching of adsorbed Dox by rGO or LHT-rGO using a fluorescence microplate reader (Gemini XS; Molecular Device).

2.6. Cellular uptake test of Dox delivered by LHT-rGO nanosheets

The cellular uptake of Dox was tested in human KB carcinoma cells using confocal microscopy. KB cells were seeded onto cover glasses at a density of 8 $\times$ 10^4cells/well in 24-well plates. The next day, cells were treated with rGO/Dox or LHT-rGO/Dox at a concentration of 10 μM Dox. After incubating for 1 h, cells were washed and fixed with 4% paraformaldehyde in PBS for 15 min, and stained with 4',6-diamidino-2-phenylindole dihydrochloride (DAPI). The fluorescence of cellular Dox was observed using a confocal laser-scanning microscope (LSM 5 Exciter; Carl Zeiss, Inc., Jena, Germany).

2.7.In vitro antitumor efficacy study of Dox-loaded nanosheets

The *in vitro* antitumor efficacy of Dox on nanosheets was tested using cell viability assays. KB cells were seeded into 48-well plates at a density of 6 $\times$ 10^4cells/well. The next day, cells were treated with rGO/Dox or LHT-rGO/Dox at a concentration of 3 μM Dox. After 1 h, culture media were replaced with fresh media and cells were maintained for 24 h. Cell viability was measured using a Cell Counting Kit-8 (CCK-8; Dojindo, Tokyo, Japan) as described by the manufacturer. Briefly, 20 μl of CCK-8 (water-soluble tetrazolium salt) solution was added to each well for 30 min, and absorbance was measured at 450 nm using a microplate reader (Sunrise-Basic TECAN, Männedorf,

Switzerland). Cell viability in each group was expressed as a percentage of that in control cells.

2. 8. In vivo molecular imaging

The *in vivo* distribution of 1,2-distearoyl-sn-glycero-3-phosphoethanolamine-N-(Alexa Fluor 680[polyethylene glycol] -5000) (DSPE-PEG5000-Alexa Fluor 680)-labeled LHT-rGO nanosheets to tumor tissues was tested by molecular imaging. Five-week-old female Balb/c and athymic nude mice (Orient Bio Inc., Seongnam, Kyonggi-do, Republic of Korea) were used for *in vivo* studies. All animals were maintained and used in accordance with the Guidelines for the Care and Use of Laboratory Animals of the Institute of Laboratory Animal Resources, Seoul National University (Seoul, Republic of Korea; approved animal experimental protocol number SNU-130129-3-1). The mice were subcutaneously inoculated at both dorsal sides with 2×10^6 KB cells. After tumors had become established, Dox (2.5 mg/kg) was intravenously administered in free form or on rGO or LHT-rGO nanosheets. After 1, 24 and 48 h, delivery efficiency was assessed using an eXplore Optix system (Advanced Research Technologies Inc., Montreal, Canada). For molecular imaging, rGO or LHT-rGO was labeled with DSPE-PEG5000-Alexa Fluor 680 by adding 10 mg DSPE-PEG5000-Alexa Fluor 680 to 2.5 mg/ml rGO or LHT-rGO. The phosphate quantification was conducted with DSPE-PEG5000-Alexa Fluor 680 labelled-rGO or LHT-rGO to confirm the interation between DSPE-PEG5000-Alexa Fluor 680 and rGO or LHT-rGO. Excitation and emission spots were raster-scanned in 1-mm steps over the region of interest to generate emission wavelength scans. A 670-nm pulsed-laser diode was used to excite Cy5.5 molecules. Long wavelength fluorescence emission (600–700 nm) was detected with a fast photomultiplier tube (Hamamatsu Photonics, Hamamatsu, Japan) and a time-correlated single photon counting system (Becker and Hickl GmbH, Berlin, Germany).

2. 9. In vivo antitumor activity test

The antitumor effects of Dox were tested in KB tumor-bearing mice. Five-week-old athymic nude mice (Orient Bio, Inc.) were subcutaneously injected at the dorsal right side with 2×10^6 KB cells. When tumor volumes reached 150–180 mm^3, mice were intravenously administered Dox and/or LHT7 in free form or on nanosheets. For systemic injection, mice were treated with Dox (1.25 mg/kg) alone or as a mixture with LHT7 (12.5 mg/kg). For comparison, mice were intravenously treated with plain rGO/Dox (2.5 mg/kg rGO, 1.25 mg/kg Dox), LHT-rGO (12.5 mg/kg LHT, 2.5 mg/kg rGO) or LHT-rGO/Dox (12.5 mg/kg LHT, 2.5 mg/kg rGO, 1.25 mg/kg Dox) nanosheets in PBS every 3 day for a total of three injections. Twenty-five days after tumor inoculation, tumor tissues were isolated and weighed, then fixed in 10% neutral buffered formalin and embedded in paraffin blocks for further histological evaluation. Tumor tissue sections (4 μm thick) were immunostained with an anti-proliferating cell nuclear antigen (PCNA) antibody (Thermo Fisher Scientific) and subjected to terminal deoxynucleotidyl transferase dUTP nick-end labeling (TUNEL) assays (Millipore Corporation, Billerica, MA, USA) to determine cell-proliferation status and apoptosis, respectively. The numbers of proliferating and apoptotic cells were counted using the image analysis software, Image-Pro Plus Version 6.0 (Media Cybernetics, Inc., Rockville, MD, USA), after photographing five different fields at a magnification of 200 using an Eclipse TE2000-S microscope (Nikon, Tokyo, Japan).

2.10. Statistics

Analysis of variance (ANOVA) with Student-Newman-Keuls post hoc tests was used for statistical evaluation of experimental data. All statistical analyses were done using SigmaStat software (version 3.5; Systat Software, Richmond, CA, USA); a p-value < 0.05 was considered significant.

3. Results

3.1. Characterization of LHT-rGO nanosheets

Surface coating of rGO by LHT7 was evaluated by monitoring the quenching of F-LHT7 by rGO (**Fig. 1a**). FITC fluorescence is "turned off" upon adhesion of F-LHT7 to rGO via the taurocholate anchoring moiety owing to the fluorescence -quenching feature of graphene nanosheets[14]. Consistent with this fluorescence-quenching phenomenon, the fluorescence intensity of FITC steadily decreased as the weight ratio of F-LHT7 to rGO decreased, a reduction interpreted as LHT7 loading onto rGO (**Fig. 1b**). At LHT7:rGO weight ratios of 1:1 and 1:5, 89.6% ± 0.2% and 75. 4% ± 0.2% of added F-LHT7 were loaded onto rGO, respectively (**Fig. 1c**). TEM imaging of rGO (**Fig. 1d**) and LHT-rGO (**Fig. 1e**) nanosheets revealed the unique shape of graphene-based nanosheets.

3.2. Dispersion stability of LHT-rGO nanosheets

LHT-rGO showed greater dispersion stability in buffers and serum than rGO nanosheets (**Fig. 2**). Immediately after dispersion of LHT-rGO in PBS, rGO and LHT-rGO nanosheets with LHT7:rGO weight ratios less than 0.5:1 exhibited aggregation. Twenty-four hours after dispersion, LHT-rGO with a LHT7:rGO weight ratio of 1:1 formed aggregates; in contrast, LHT-rGO with LHT7:rGO weight ratios greater than 5:1 exhibited a stable dispersion at 24 h (**Fig. 2a**) that was maintained up to 3 d (data not shown). Moreover, LHT-rGO nanosheets with a LHT7:rGO weight ratio of 5:1 were stable in RPMI media supplemented with 10%, 50% or 90% FBS (**Fig. 2b**). Thus, a LHT7:rGO weight ratio of 5:1 was chosen for further experiments.

3.3. Loading of Dox onto LHT-rGO nanosheets

The Dox loading capacity of rGO and LHT-rGO nanosheets was evaluated by monitoring fluorescence quenching of Dox. Fluorescence quenching of Dox by rGO or LHT-rGO, manifesting as a decrease in fluorescence intensity, was

greater at lower levels of added Dox and decreased as the amount of added Dox exceeded the loading capacity of the nanosheets (**Fig. 3**). LHT-rGO nanosheets showed a higher capacity for Dox loading compared with rGO nanosheets (**Fig. 3a**). At Dox:rGO weight ratios of 1:1, 2:1 and 5:1, almost complete quenching of Dox fluorescence (~90%) was observed with LHT-rGO nanosheets (**Fig. 3b**). In contrast, fluorescence quenching by rGO was only 73.1% ± 2.1% at a Dox:rGO ratio of 1:1—indicating that the loading capacity of rGO was exceeded even at the lowest level of added Dox—and was further diminished at ratios of 2:1 (47.2% ± 0.8%) and 5:1 (23.7% ± 0.8%) (**Fig. 3c**). Dox-loaded LHT-rGO nanosheets are depicted in Fig. 3d.

3.4. Cellular uptake and anticancer efficacy of Dox delivered on LHT-rGO nanosheets

Dox on both plain rGO (rGO/Dox; **Fig. 4c**) and LHT-rGO (LHT-rGO/Dox; **Fig. 4d**) was effectively taken up by KB cells, as evidenced by direct detection of intracellular Dox fluorescence. These results were confirmed in experiments using rGO nanosheets labeled with DSPE-PEG5000-Alexa Fluor 680, which showed similar cellular uptake of rGO/Dox (**Fig. 4e**) and LHT-rGO/Dox (**Fig. 4f**). Merged fluorescence images of DAPI, Dox and DSPE-PEG5000-Alexa Fluor 680-labeled rGO (**Fig. 4g**) or DSPE-PEG5000-Alexa Fluor 680-labeled LHT-rGO (**Fig. 4h**) revealed that Dox and rGO differed in the intracellular distribution. Dox was co-localized to the nucleus. whereas rGO or LHT-rGO was observed in the cytoplasm. Consistent with the results of cellular uptake experiments, the *in vitro* anticancer efficacy did not significantly differ between the two preparations, with LHT-rGO/Dox and rGO/Dox reducing KB cell viability to 38.9% ± 1.0% and 40.2% ± 1.6%, respectively (**Fig. 4i**).

3.5. In vivo tumor tissue distribution of LHT-rGO/Dox

We next evaluated the tumor distribution of LHT-rGO/Dox and rGO/Dox following *in vivo* administration. At 1 h after dosing, the distribution at tumor sites was greater in LHT-rGO/Dox-treated mice than in rGO/Dox-treated mice

(**Fig. 5a**), a difference that was maintained at 24 and 48 h post dose. At 48 h post dose, photon count measurements revealed that the tumor retention of LHT-rGO/Dox was 7-fold higher than that of rGO/Dox (**Fig. 5b**).

3.6. In vivo antitumor effects of LHT-rGO/Dox

The *in vivo* antitumor efficacy of LHT-rGO/Dox was evaluated in a KB tumor xenograft model. On day 25 after tumor inoculation, tumor volume was smaller in mice treated with LHT-rGO/Dox than in those treated with free LHT7, Dox, or rGO/Dox (**Fig. 6a**). Consistent with this, tumor weights on day 25 were lowest in mice treated with LHT-rGO/Dox, which showed a 92.5% ± 3.1% reduction in tumor weight compared with untreated mice (**Fig. 6b**).

The density of proliferating cells was proportional to the tumor volume and was lowest in mice treated with LHT-rGO/Dox (**Fig. 7a and c**). Moreover, although the number of apoptotic cells was significantly enhanced in all drug-treated groups compared to the control, the LHT-rGO/Dox-treated group showed the highest number of apoptotic cells. Compared to mice treated with a mixture of free LHT and Dox, the group treated with LHT-rGO/Dox showed a 2.4-fold increase in the number of apoptotic cells (**Fig. 7b and d**). Collectively, these results indicate that the antitumor activity of Dox was enhanced by delivery on LHT-rGO nanosheets.
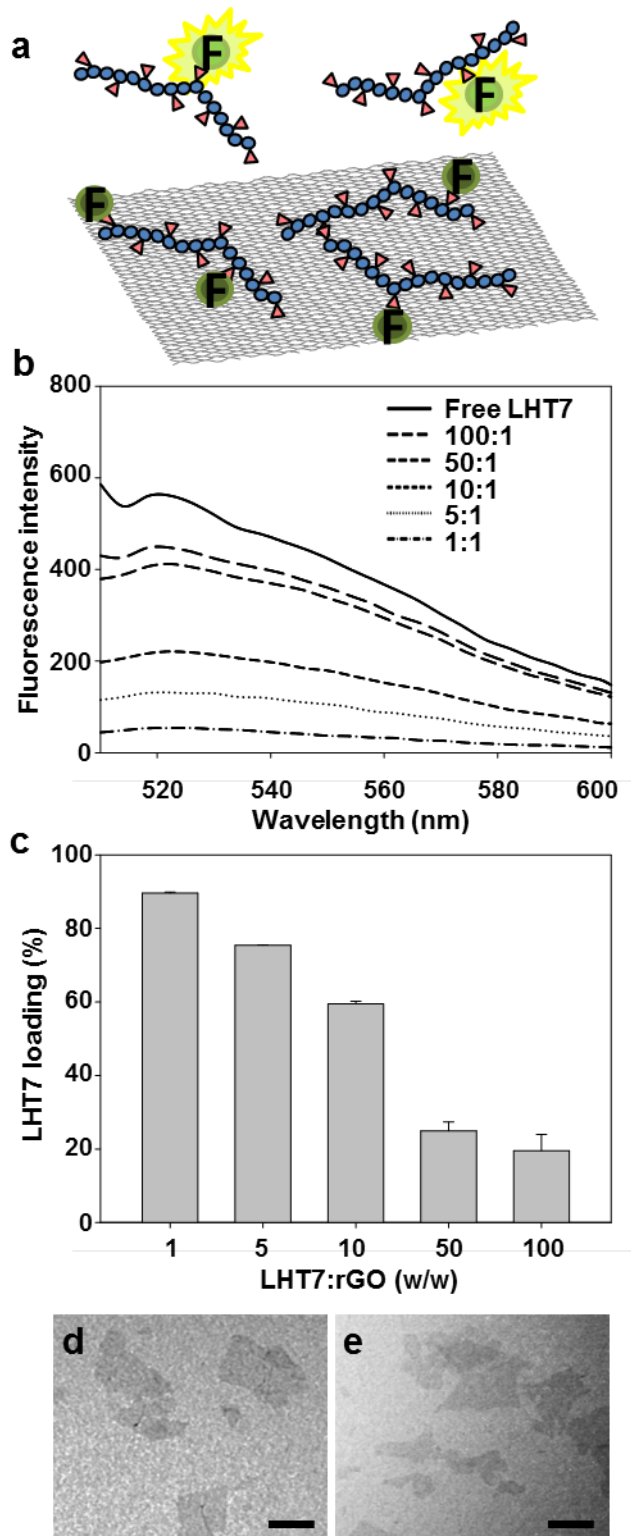
Figure 1. Characterization of LHT7-rGO nanosheets. F-LHT7 adheres to rGO nanosheets, triggering fluorescence quenching (a). Interactions between rGO and F-LHT7 were analyzed by fluorometry (b), and the loading efficiency of F-LHT7 onto rGO was measured (c) at various weight ratios (n = 4). TEM images of uncoated rGO (d) and LHT-rGO (e) in which LHT was coated onto rGO at a 5:1 w/w ratio (e). Scale bar = 100 nm.
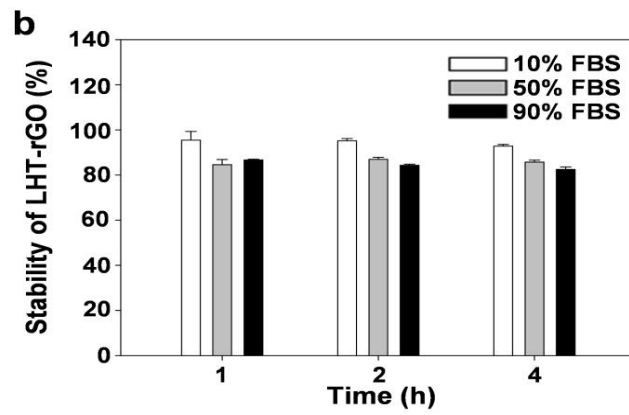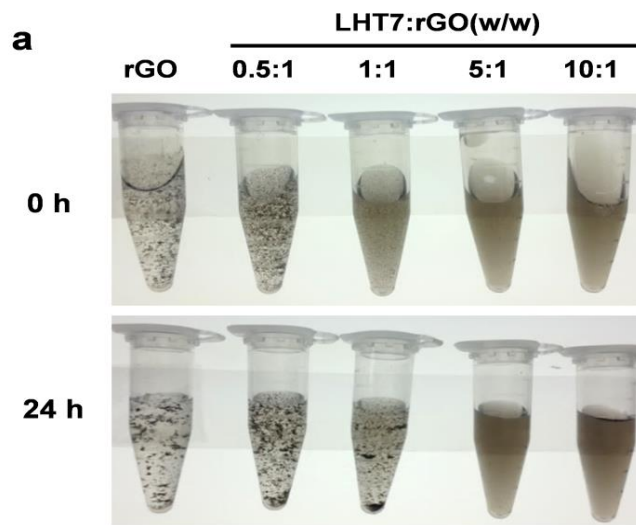
a

LHT7:rGO(w/w)

| rGO | 0.5:1 | 1:1 | 5:1 | 10:1 |

0 h

24 h

b

- 13 -

Figure 2. Dispersion stability of LHT-rGO nanosheets in PBS and culture media. The stability of rGO and LHT-rGO nanosheet suspensions was evaluated in PBS (a). LHT-rGO with 5:1 w/w ratio was dispersed in RPMI media supplemented with 10%, 50% or 90% FBS (b).
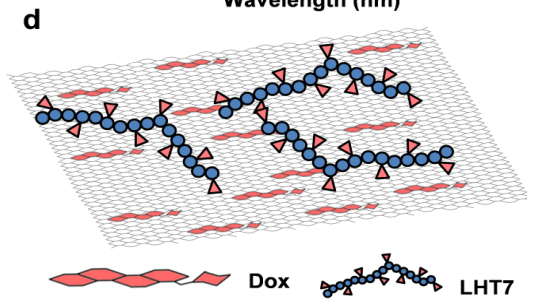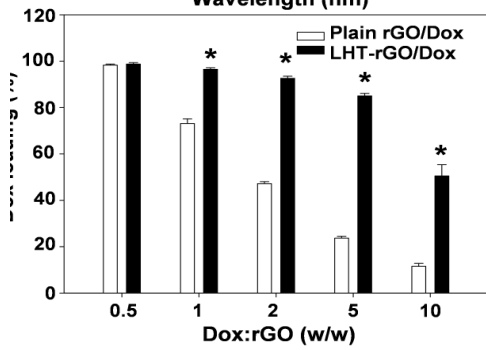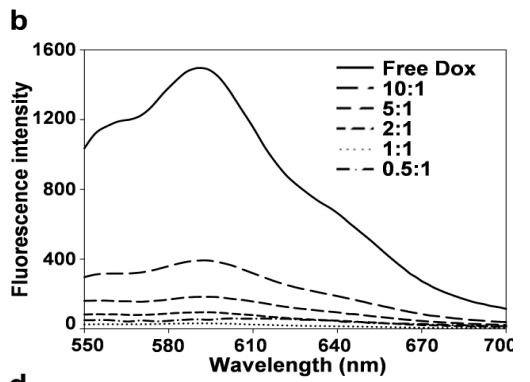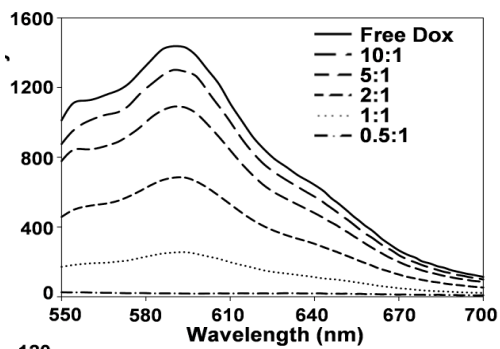
b

d

Figure 3. Loading of Dox onto rGO or LHT-rGO nanosheets. Dox was loaded onto rGO (a) and LHT-rGO (b) nanosheets. Interactions between rGO or LHT-rGO and Dox were analyzed by fluorescence spectroscopy at various Dox:rGO weight ratios. The loading efficiency of Dox in complexes with rGO or LHT-rGO was measured (c). A schematic illustration of LHT-rGO/Dox is shown (d). (*$p < 0.05$ compared to the rGO group; t-test.)
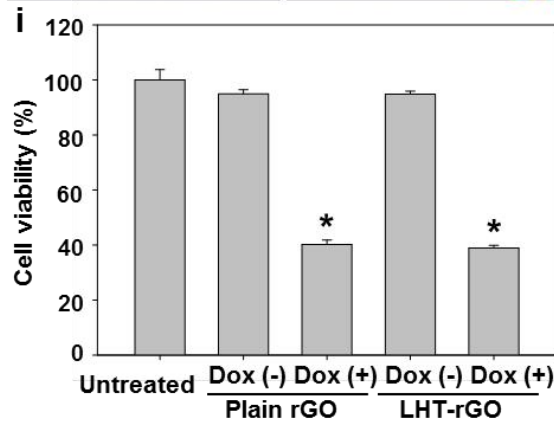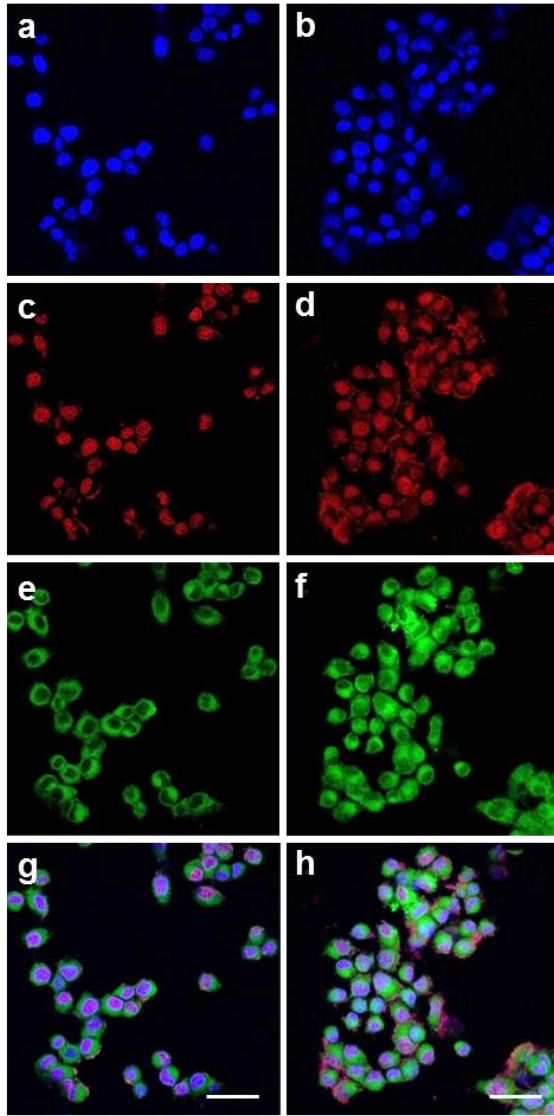
Figure 4. Cellular uptake and antitumor effect of Dox delivered by nanosheets. KB cells were treated with Dox loaded onto rGO or LHT-rGO (plain or DSPE-PEG5000-Alexa Fluor 680-labeled). One hour after treatment, the fluorescence of DAPI stained on rGO/Dox (a) or LHT-rGO/Dox (b)-treated cells, Dox delivered on rGO (c) or LHT-rGO (d), the fluorescence of rGO (e) or DSPE-PEG5000- Alexa Fluor 680-labeled LHT-rGO (f), and the merged fluorescences of DSPE-PEG5000-Alexa Fluor 680-labeled rGO/Dox (g) or DSPE-PEG5000-Alexa Fluor 680-labeled LHT-rGO/Dox (h) were observed by confocal microscopy. Scale bar = 20 μm. (i) For assessment of cancer cell killing effects, KB cells were treated with rGO or LHT-rGO, with or without Dox, and cell viability was quantified by CCK-8 assay (n = 4). (*$p < 0.05$ compared to untreated, rGO/Dox, and LHT-rGO/Dox groups; ANOVA and Student-Newman-Keuls test.)

a

Time (h)

| 1 | 24 | 48 |

Untreated

Plain rGO /Dox

LHT-rGO / Dox

1.02e+004   7.83e+003   5.44e+003   3.05e+003   665

Intensity(NC)

b

Photon counts at tumor site (x10³)

□ Plain rGO/Dox
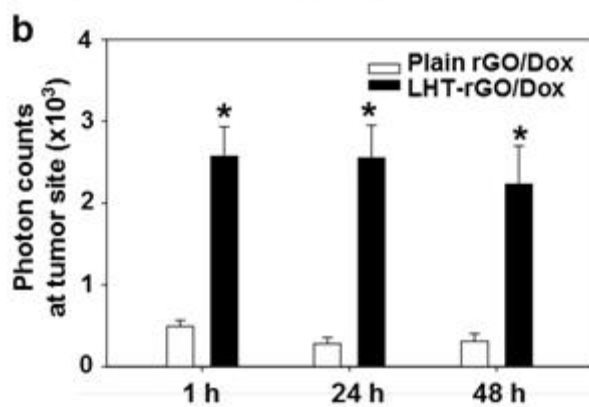■ LHT-rGO/Dox

1 h   24 h   48 h
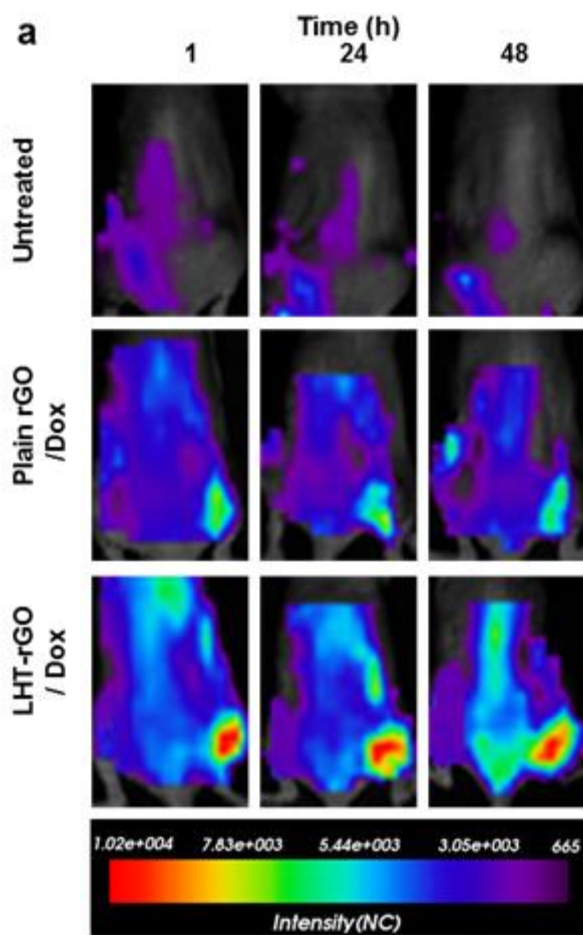
Figure 5. *In vivo* biodistribution of LHT-rGO/Dox. KB tumor-bearing mice were intravenously administered 2.5 mg of Dox on rGO, or on LHT-rGO. For molecular imaging, both rGO and LHT-rGO were labeled with DSPE-PEG5000-Alexa Fluor 680. (a) At different times post injection (1, 24 and 48 h), the *in vivo* distribution of rGO/Dox and LHT-rGO/Dox was visualized using a molecular imaging system. (b) Quantification of average photon counts at the tumor site (n = 4). (*p < 0.05 compared to the rGO/Dox group; t-test.)

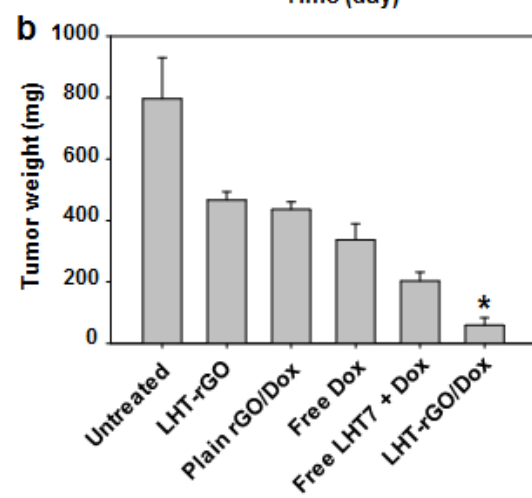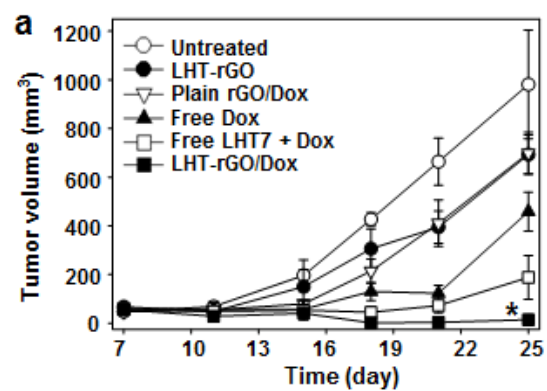**Figure 6.** *In vivo* antitumor efficacy of LHT-rGO/Dox. KB tumor-bearing mice (5 mice/group) were intravenously injected with Dox alone, a mixture of free Dox and LHT7, rGO/Dox or LHT-rGO/Dox (2.5 mg/kg Dox) in PBS every 3 day beginning on day 7. Tumor volumes were measured for each group (a). On day 25, tumor tissues were excised and weighed (B). (*p < 0.05 compared to other groups; ANOVA and Student-Newman-Keuls test)
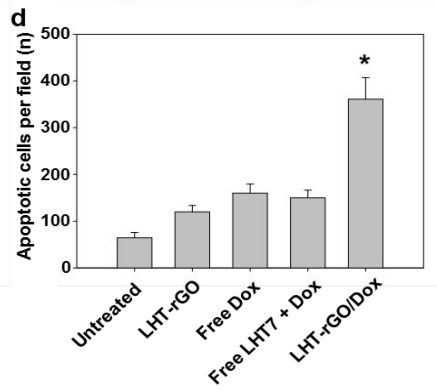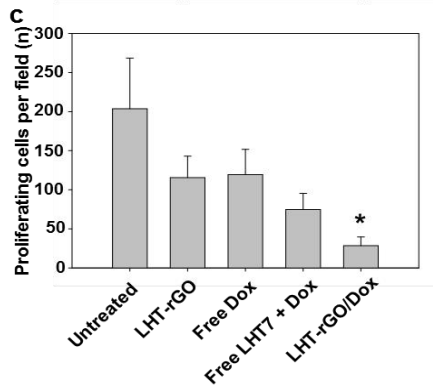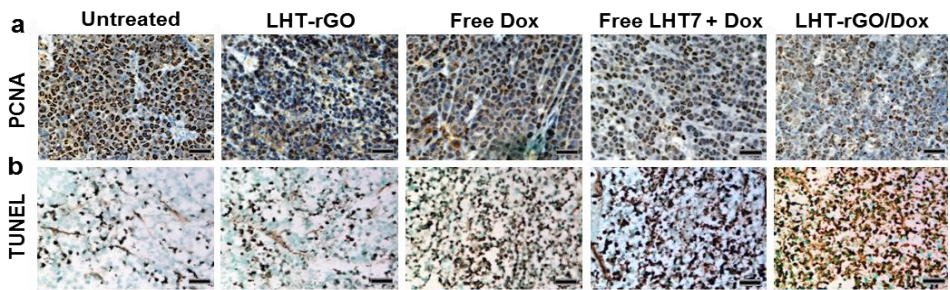
Figure 7. Immunohistochemistry of tumor tissues. Tumor tissues were excised and sectioned for anti-PCNA antibody immunostaining (a) and TUNEL assay (b). The numbers of PCNA-immunostained proliferating cells (c) and TUNEL-labeled apoptotic cells (d) in isolated tumor tissues were determined (n = 4; *p < 0.05 compared to other groups; ANOVA and Student-Newman-Keuls test). Scale bar = 100 μm.

4. Discussion

This study demonstrated that rGO coated with anti-angiogenic anticancer LHT7 is a much more effective alternative to rGO nanosheets for enhanced delivery of anticancer drugs to tumors. The coating of rGO with LHT7 improved physicochemical properties such as dispersion stability and Dox-loading capacity as compared with rGO nanosheets.

LHT-rGO was prepared by physical adsorption of LHT-7 onto rGO nanosheets. LHT7 was synthesized by conjugating the amine group of sodium ethylenediamine taurocholate with the carboxylic groups of LMWH at a molar ratio of 1 to 7[17,18]. The sterane core of LHT7 belongs to the class of 4-cyclic compounds derived from steroids or sterols. The sterane core structure is known to confer binding affinity to rGO via hydrophobic interactions[20]. Thus, the seven-sterane structure of LHT7 conferred by taurocholate is expected to anchor LHT7 to rGO via hydrophobic interactions.

Surface modification with LHT-7 might also account for the greater dispersion stability of LHT-rGO nanosheets compared with rGO nanosheets (**Fig. 2**). It has previously been reported that coating of graphene nanosheets with unfractionated heparin increases their dispersion in water and enhances the anticoagulant activity of heparin[21]. Although LHT-7 is derived from LMWH, LHT-7 differs from LMWH from the perspective of anticoagulant activity. Unlike LMWH, LHT-7 has been found to have little anticoagulant activity[18]. This lack of coagulant activity is desirable from the standpoint of using LHT-7 as a coating material for rGO nanosheets.

In this study, we separated rGO/Dox and LHT-rGO/Dox from free Dox using a desalting column. To test whether there was physical adsorption of rGO/Dox and LHT-rGO/Doxon the desalting column, we measured the UV spectrum of rGO/Dox and LHT-rGO/Dox after single and double elution through the desalting column. The similar UV absorbance spectra of single eluted and double-eluted rGO/Dox and LHT-rGO/Dox support that the physical adsorption of rGO/Dox or LHT-rGO/Dox onto the desalting column was negligible.

LHT-rGO nanosheets allowed higher Dox loading capacity compared with rGO nanosheets (**Fig. 3c**). Dox has been reported to bind graphene-based nanosheets and has been used as a model drug for pharmaceutical applications of graphenes[22-25]. While this affinity for graphene-based nanosheets enables Dox to bind uncoated rGO, the highly negatively charged LHT7 on LHT-rGO nanosheets may further bind positively charged Dox through electrostatic interaction, thereby increasing Dox loading capacity. Indeed, we recently reported increased loading efficiency of Dox on negatively charged hyaluronic acid-coated rGO via additional electrostatic interactions[14].

For *in vivo* visualization the biodistribution of LHT-rGO nanosheets, we used DSPE-PEG5000-Alexa Fluor 680 as an imaging probe. The DSPE lipid moiety of the probe was used to anchor the probe onto rGO nanosheets via hydrophobic interaction. The attachment of DSPE-PEG5000-Alexa Fluor 680 onto rGO nanosheets was tested by the content of phosphate on rGO. After incubation of DSPE-PEG5000-Alexa Fluor 680 with rGO, the content of unattached DSPE-PEG5000-Alexa Fluor 680 in the supernatant was measured by the phosphate amount of DSPE. More than 98% of DSPE-PEG5000-Alexa Fluor 680 in the supernatant. Moreover, there was no difference in the loading efficiencies between rGO/Dox and LHT-rGO/Dox with the fluorescent lipid probe. Similar to this study, previous studies have used fluorescent lipid markers for *in vivo* imaging of graphenes[26,27].

It is notable that the enhanced anti-tumor effect of LHT-rGO/Dox over plain rGO/Dox was observed *in vivo* (**Fig. 6**), but not *in vitro* (**Fig. 4**). Consistent to the *in vitro* anti-tumor activity, the cellular uptake patterns did not differ between LHT-rGO/Dox and rGO/Dox. The discrepancy between *in vitro* and *in vivo* anti-tumor effect of LHT-rGO/Dox might be explained by the working mechanisms of LHT7. LHT7 has been reported to exert its anticancer effect by binding with angiogenic growth factors, such as vascular endothelial growth factor, that are highly expressed in tumor tissue environment[18]. Since the concentrations of angiogenic growth factors would be much lower in the cell culture medium as compared to the tumor microenvironment *in vivo*, LHT7-

rGO/Dox might have little interaction with the growth factors. Such lack of interaction could have resulted in lack of synergistic anticancer effects with Dox in the cell culture system.

After cellular uptake of Dox-loaded rGO or LHT-rGO nanosheets, nucleus accumulation of Dox (**Fig. 4c, d**) was observed while rGO remained in cytoplasm (**Fig. 4e, f**). The nucleus localization of fluorescent Dox indicates that Dox might be liberated from rGO nanosheets. After loading onto rGO nanosheets, quenching of Dox was observed. The recovery of fluorescence intensity of Dox in the cell nucleus would be the result of dissociation of Dox from rGO in endolysosomes and diffusion of the liberated Dox from endolysosomes to the cytoplasm and finally to the liberated Dox from endolysosomes to the cytoplasm and finally to the nucleus. In a recent study, the release of Dox from GO nanosheets in the living cells was indeed observed by surface-enhanced Raman spectroscopy[28]. In the study, they reported that Dox was first liberated from GO nanosheets and escaped to the cytoplasm, and finally translocated to the nucleus. Unlike Dox, they observed that GO nanosheets were trapped in the cytoplasm. The retention of GO nanosheets in cytoplasm is possibly due to the size limitation of nuclear pore (less than 9 nm). Gold nanoparticles of 6 nm size were reported to be distributed to the nucleus of the cancer cells, whereas gold nanoparticles of 15 nm were shown to stay in the cytoplasm without entering the nucleus[29].

We observed the higher tumor tissue distribution of LHT-rGO/Dox compared with rGO/Dox. The enhanced tumor tissue distribution of LHT-rGO/Dox over rGO/Dox might be in part attributed to the enhanced stability of LHT-rGO/Dox in serum (**Fig. 2b**).

This enhanced tumor tissue distribution and retention of LHT-rGO/Dox (**Fig. 5**) translated into significantly improved antitumor efficacy in KB tumor-bearing mice compared with rGO/Dox (**Fig. 6**). TUNEL assays showed that the population of apoptotic cells was highest in tumor tissues of LHT-rGO/Dox-treated mice (**Fig. 7b**), suggesting that apoptosis is likely the main mechanism by which LHT-rGO/Dox produces its antitumor effects. It is also possible that

the anti-angiogenic anticancer activity of LHT7 on rGO could contribute to the enhanced antitumor activity. Indeed, LHT7 has been shown to bind angiogenic growth factors, like VEGF, and serve as a potential anti-angiogenic anticancer drug[18]. Moreover, liposomal co-delivery of LHT7 with an anticancer drug has been shown to produce a synergistic effect[19].

The greater antitumor effect of LHT-rGO/Dox compared with a mixture of free LHT7 and Dox underscores the importance of nanocarriers in chemotherapy. Recently, dendronized heparin-Dox conjugate-based nanoparticles were shown to exert improved antitumor activity in a 4T1 breast tumor model[30]. Compared with chemical conjugation of Dox, the physical adsorption of Dox onto LHT-rGO may have advantages. First, the absence of chemical modifications of the Dox structure may eliminate efficacy and safety concerns raised for chemically modified drugs. Moreover, the additional chemical conjugation step may increase nanomedicine manufacturing costs.

5. Conclusion

The surface coating of rGO with LHT7, a LMWH derivative with anti-angiogenic anticancer property, increased the dispersion stability of rGO in serum and enhanced its Dox-loading capacity through additional electrostatic interaction. Following systemic administration, LHT-rGO/Dox exhibited greater and more prolonged distribution to tumor tissues compared with rGO/Dox. Moreover, LHT-rGO/Dox effectively diffused into the tumor tissues and exerted enhanced antitumor effects. Collectively, our results support the potential application of LHT-rGO for the delivery of various anticancer drugs.

References

1   J. Liu, L. Cui, D. Losic, Graphene and graphene oxide as new nanocarriers for drug delivery applications, Acta Biomater. 9 (2013) 9243-9257.

2   L. Feng, L. Wu, X. Qu, New horizons for diagnostics and therapeutic applications of graphene and graphene oxide, Adv. Mater. 25 (2013), 168-186.

3   K. Yang, L. Feng, X. Shi, Z. Liu, Nano-graphene in biomedicine: theranostic applications, Chem. Soc. Rev. 2013, 42 (2013) 530-547.

4   M.C. Duch, G.R.S. Budinger, Y.T. Liang, S. Soberanes, D. Urich, S.E. Chiarella, et al., Minimizing oxidation and stable nanoscale dispersion improves the biocompatibility of graphene in the lung, Nano Lett. 11 (2011) 5201-5207.

5   H. Ali-Boucetta, D. Bitounis, R. Raveendran-Nair, A. Servant, J. Van den Bossche, K. Kostarelos, Graphene oxide: purified graphene oxide dispersions lack *in vitro* cytotoxicity and *in vivo* pathogenicity, Adv. Healthc. Mat. 2 (2013) 433-441.

6   H.Y. Mao, S. Laurent, W. Chen, O. Akhavan, M. Imani, A.A. Ashkarran, et al., Graphene: promises, facts, opportunities, and challenges in nanomedicine Chem. Rev. 113 (2013) 3407-3424.

7   B.J. Hong, O.C. Compton, Z. An, I. Eryazici, S.T. Nguyen, Successful stabilization of graphene oxide in electrolyte solutions: enhancement of biofunctionalization and cellular uptake, ACS Nano 6 (2012) 63-73.

8   M. Lotya, P.J. King, U. Khan, S. De, J.N. Coleman, High-concentration, surfactant-stabilized graphene dispersions, ACS Nano 4(2010) 3155-3162.

9   S. Lin, C.J. Shih, M.S. Strano, D. Blankschtein, Molecular Insights into the surface morphology, layering structure, and aggregation kinetics of surfactant-stabilized graphene dispersions, J. Amer. Chem. Soc. 133(2011) 12810-12823.

10 C. Hou, H. Quan, Y. Duan, Q. Zhang, H. Wang, Y. Li, Facile synthesis of water-dispersible Cu2Onanocrystal-reduced graphene oxide hybrid as a promising cancer therapeutic agent, Nanoscale 5 (2013) 1227-1232.

11 K. Yang, L. Feng, H. Hong, W. Cai, Z. Liu, Preparation and functionalization of graphene nanocomposites for biomedical applications, Nat. Protoc. 8 (2013) 2392-2403.

12 L. Zhang, Z. Wang, Z. Lu, H. Shen, J. Huang, Q. Zhao, et al. PEGylated reduced graphene oxide as a superior ssRNA delivery system, Mat. Chem. B. 1 (2013) 749-755.

13 H. Kim, D. Lee, J. Kim, T.I. Kim, W.J. Kim, Photothermally triggered cytosolic drug delivery via endosome disruption using a functionalized reduced graphene oxide, ACS Nano 7 (2013) 6735-6746.

14   W. Miao, G. Shim, C.M. Kang, S. Lee, Y.S. Choe, H.G. Choi, et al., Cholesteryl hyaluronic acid-coated, reduced graphene oxide nanosheets for anti-cancer drug delivery, Biomaterials 34 (2013) 9638-9647.

15   Y.K. Kim, M.H. Kim, D.H. Min, Biocompatible reduced graphene oxide prepared by using dextran as a multifunctional reducing agent, Chem. Commun. 47 (2011) 3195-3197.

16   Y. Wang, P. Zhang, C. Fang, C. Liu, L. Zhan, Y.F. Li, et al., Green and easy synthesis of biocompatible graphene for use as an anticoagulant, RSC Adv. 2 (2012) 2322-2328.

17   E. Lee, Y.S. Kim, S.M. Bae, S.K. Kim, S. Jin, S.W. Chung, et al., Polyproline-type helical-structured low-molecular weight heparin (LMWH)-taurocholate conjugate as a new angiogenesis inhibitor, Int. J. Cancer 124 (2009) 2755-2765.

18   S.W. Chung, M. Lee, S.M. Bae, J. Park, O.C. Jeon, H.S. Lee, Potentiation of anti-angiogenic activity of heparin by blocking the ATIII-interacting pentasaccharide unit and increasing net anionic charge, Biomaterials 33 (2012) 9070-9079.

19   J.Y. Kim, G. Shim, H.W. Choi, J. Park, S.W. Chung, S. Kim, et al., Tumor vasculature targeting following co-delivery of heparin-taurocholate conjugate and suberoylanilide hydroxamic acid using cationic nanolipoplex, Biomaterials 33 (2012) 4424-4430.

20   M. Swierczewska, K.Y. Choi, E.L. Mertz, X. Huang, F. Zhang, L. Zhu, et al., A facile, one-step nanocarbon functionalization for biomedical applications, Nano Lett. 12 (2012) 3613-3620.

21   D.Y. Lee, Z. Khatun, J.H. Lee, Y.K. Lee, I. In, Blood compatible graphene/heparin conjugate through noncovalent chemistry, Biomacromolecules 12 (2011) 336-341.

22   G. Liu, H. Shen, J. Mao, L. Zhang, Z. Jiang, T. Sun, et al., Transferrin modified graphene oxide for glioma-targeted drug delivery: *in vitro* and *in vivo* evaluations, ACS App. Mater. Inter. 5 (2013) 6909-6914.

23   W. Miao, G. Shim, S. Lee, Y.S. Choe, Y.K. Oh, Safety and tumor tissue accumulation of pegylated graphene oxide nanosheets for co-delivery of anticancer drug and photosensitizer, Biomaterials 34 (2013) 3402-3410.

24   Y. Wang, R. Huang, G. Liang, Z. Zhang, P. Zhang, S. Yu, et al., MRI-visualized, dual-targeting, combined tumor therapy using magnetic graphene-based mesoporous silica, Small 10 (2013) 109-116.

25   F. Wang, B. Liu, A.C. Ip, J. Liu, Orthogonal adsorption onto nano-graphene oxide using different intermolecular forces for multiplexed delivery, Adv. Mater. 25 (2013) 4087-4092.

26   C. Peng, W. Hu, Y. Zhou, C. Fan, Q. Huang, intracellular imaging with a graphene-based fluorescent probe, small 6 (2010) 1686-1692.

27 J.T. Robinson, S.M. Tabakman, Y. Liang, H. Wang, H.S. Casalongue, D. Vinh, et al., Ultrasmall reduced graphene oxide with high near-infrared absorbance for photothermal therapy, J. Am. Chem. Soc. 133 (2011) 6825-6831.

28 J. Huang, C. Zong, H. Shen, Y. Cao, B. Ren, Z. Zhang, Tracking the intracellular drug release from grapheme oxide using surface-enhanced raman spectroscopy, Nanoscale 5 (2013) 10591-10598.

29 K. Huang, H. Ma, J. Liu, S. Huo, A. Kumar, T. Wei, et al., Size-dependent localization and penetration of ultrasmall gold nanoparticles in cancer cells, multicellular spheroids, and tumors *in vivo*, ACS Nano 6 (2012) 4483-4493.

30 W. She, N. Li, K. Luo, C. Guo, G. Wang, Y. Geng, et al., Dendronized heparin−doxorubicin conjugate based nanoparticle as pH-responsive drug delivery system for cancer therapy, Biomaterials 34 (2013) 2252-2264.

초 록

표면수식 그래핀 나노시트를 이용한 항암제 전달 연구

한정훈

분자의학 및 바이오제약학과

융합과학기술대학원

서울대학교

본 연구에서는 항암제 전달 연구를 위한 나노 전달체로서 항 신생혈관 기능이 있는 토우콜레이트와 저분자량 헤파린의 접합체 (LHT7)로 표면을 수식한 환원형 그래핀 나노시트 (reduced graphene oxide; rGO)를 소개하고 있다. rGO 표면에 LHT7 를 이용한 표면수식은 형광 표지된 LHT7 를 이용하여 rGO 에 의한 형광 소거 효과를 관찰함으로써 확인하였다. 표면수식을 하지 않은 rGO 와는 달리, LHT7 을 이용하여 표면수식한 rGO (LHT-rGO) 는 생리학상의 조건에서 적어도 24 시간 이상 안정한 분산성을 유지하며 rGO 에 비해 항암의약 독소루비신 (Dox)의 탑재량이 더 높은 것으로 관찰되었다. 종양이 형성된 마우스에 정맥 주사한 후 생체 내 조직 분포도를 측정한 결과, Dox 를 탑재한 LHT-rGO 의 종양분포가 LHT7 을 코팅하지 않은 rGO 에 Dox 를 탑재한 그룹보다 7 배 가량 높았으며 종양의 크기는 미처리군과 비교했을 때 92.5 % ± 3.1 % 까지 줄어드는 것을 확인하여 Dox 단독처리군과 Dox 탑재 rGO 군과 비교하였을 때 높은 항암효과를 나타내었다. 또한, TUNEL assay 의 결과로 LHT-rGO 에 Dox 를

탑재한 그룹에서 세포자살이 가장 많이 일어난 것을 확인할 수 있었다. 이러한 결과들은 LHT-rGO 의 혈중 분산성, 약물 탑재능력, 세포자살을 일으켜 항암 효과를 일으켰으며, LHT-rGO 의 이러한 특징들은 전신 투여시 종양 조직으로 항암제의 분포도를 증가시켜서 항암 효능의 증가를 가져온 것으로 보인다. LHT-rGO 는 향후에 다른 항암제들의 종양 조직 전달에도 유용하게 사용될 수 있을 것으로 기대된다.

Key words: 항신생혈관 저분자량 헤파린 유도체, 환원형 그래핀 나노시트, 분산 안정성, 독소루비신, 항암 효과